The Astrophysical Journal, 752:155 (10pp), 2012 June 20 doi:10.1088/0004-637X/752/2/155

ON PLASMA ROTATION AND DRIFTING SUBPULSES IN PULSARS: USING ALIGNED PULSAR B0826−34 AS A VOLTMETER

J. van Leeuwen[1,5] and A. N. Timokhin[2,3,4,5,6]
[1] Netherlands Institute for Radio Astronomy (ASTRON), Postbus 2, 7990 AA Dwingeloo, The Netherlands; leeuwen@astron.nl
[2] Astrophysics Science Division, NASA/Goddard Space Flight Center, Greenbelt, MD 20771, USA; andrey.timokhin@nasa.gov
[3] Astronomy Department, University of California at Berkeley, Berkeley, CA 94720, USA
[4] Sternberg Astronomical Institute, Moscow State University, Universitetskij Pr. 13, 119992 Moscow, Russia
Received 2012 January 16; accepted 2012 April 20; published 2012 June 6

ABSTRACT

We derive the exact drift velocity of plasma in the pulsar polar cap, in contrast to the order-of-magnitude expressions presented by Ruderman & Sutherland and generally used throughout the literature. We emphasize that the drift velocity depends *not on the absolute value*, as is generally used, but on the *variation* of the accelerating potential across the polar cap. If we assume that drifting subpulses in pulsars are indeed due to this plasma drift, several observed subpulse-drift phenomena that are incompatible with the Ruderman & Sutherland family of models can now be explained: we show that variations of drift rate, outright drift reversals, and the connection between drift rates and mode changes have natural explanations within the frame of the "standard" pulsar model, when derived exactly. We apply this model for drifting subpulses to the case of PSR B0826−34, an aligned pulsar with two separate subpulse-drift regions emitted at two different colatitudes. Careful measurement of the changing and reversing drift rate in each band independently sets limits on the variation of the accelerating potential drop. The derived variation is small, $\sim 10^{-3}$ times the vacuum potential drop voltage. We discuss the implications of this result for pulsar modeling.

Key words: magnetic fields – pulsars: general – pulsars: individual (PSR B0826-34) – stars: neutron

1. INTRODUCTION

Drifting subpulses are a modulation of the main pulsations seen in radio pulsars. Several months after the pulsar discovery announcement by Hewish et al. (1968), this fast variation, or second periodicity, was already reported. By this time, the original suggestion that the pulsar's main periodicity originated from stars that pulsated competed with models of neutron stars (NSs) that rotated. Thus, the detection by Drake & Craft (1968) of the "class two effect," a much faster second periodicity (∼10 ms) within the ∼1 s main period, was originally interpreted as a sign of a fast stellar pulsation, modulated by the slower stellar rotation. Yet the amount of variation seen within this second periodicity was larger than was generally expected for NS pulsations. In two papers, Don Backer (1970a, 1970b) showed that the "marching subpulses," as they were by now called, change period throughout the main pulse window, making stellar pulsations less likely but favoring magnetospheric interpretations.

This pulsar magnetosphere is filled with dense plasma, and the electric field is shielded almost everywhere. Only in some geometrically small regions is it not; there the electric field parallel to the magnetic field is capable of accelerating charged particles. Such is the current radio-pulsar "standard model," often called the force-free model, first introduced by Goldreich & Julian (1969), that we will refer to throughout this paper. It agrees very well with observational properties of pulsars: pulse peaks in both radio and gamma rays are very narrow, indicating small emitting regions and hence small regions of particle acceleration. In regions of closed magnetic field lines the plasma is trapped; but plasma around open magnetic field lines flows away, forming the pulsar wind, and needing constant replenishment.

This dense plasma consists mainly of electrons and positrons (Sturrock 1971) and is created in small regions with strong, accelerating electric fields. There is compelling observational evidence of ongoing generation of electron–positron plasma: pulsars stop emitting in radio roughly where their parameters drop below the threshold for pair creation, and observations of pulsar wind nebulae indicate they are fed by flows of dense plasma. The most plausible place for pair creation is the region of open magnetic field lines in the pulsar polar cap (Ruderman & Sutherland 1975; Scharlemann et al. 1978; Daugherty & Harding 1982). This might not be the only place of pair production in the pulsar magnetosphere (cf. Cheng et al. 1976), but without pair production in the polar cap it is difficult to imagine how the "standard model" can work. Thus, the existence of an accelerating region in the pulsar polar cap is an integral part of the "standard model."

Plasma fills the whole closed magnetic field-line zone and co-rotates with the NS. Dense plasma in the open magnetic field lines, however, exists only above the accelerating region: the region with screened electric field where magnetic field lines are frozen into the plasma is separated from the NS by an accelerating region with a strong electric field. Now, the existence of this accelerating region in general causes rotation of plasma relative to the NS. As pulsar emission is most likely generated by the plasma in the region of open magnetic field, the power spectrum of that emission must have a feature due to this plasma rotation relative to the NS. We wish to emphasize that this is a general statement that does not depend on any particular model of pulsar radio emission. If, more specifically, "stable" emitting features exist in the plasma, such as current filaments or spark columns (Ruderman & Sutherland 1975), then these will manifest as subpulses drifting across the pulse profile.

There are alternative models for the drifting subpulses, not explicitly involving plasma rotation relative to the NS; a concise review can be found in Kuijpers (2009). Some of these (e.g., Gogoberidze et al. 2005; Clemens & Rosen

[5] Both authors contributed equally.
[6] NASA Postdoctoral Program Senior Fellow.

2004) rely on some sort of standing wave pattern; the beating of the wave period with the rotational period of the pulsar provides a slow drift of emission features. In such models there are no distinct physical features actually moving relative to the star. However, fluctuation spectra for PSR B0943+10 have revealed symmetrical sidebands around its main phase modulation feature, indicative of an amplitude modulation every 20 drift bands (Deshpande & Rankin 1999); the most natural explanation is the existence of actual long-lived emitting columns in the pulsar polar cap, columns that rotate relative to the NS. The model of Fung et al. (2006) suggests that a diocotron instability due to differential rotation of plasma gives rise to plasma columns in the open magnetic field line zone. These rotate relative to the NS, but with an angular velocity that is generally different from the angular velocity of the bulk plasma rotation. Although the current-density profiles considered in Fung et al. (2006) are not directly related to existing pulsar models, in our opinion the proposed mechanism should be studied in more detail in the future.

In this paper, we consider the general idea that drifting subpulses are caused by plasma drift relative to the NS. Such plasma rotation in the open field line region is an integral part of the standard model. Our goal is not to establish a detailed model for drifting subpulses, but rather to explore testable predictions that can be made under such general assumptions about the origin of subpulse drift. We do not specify a particular mechanism leading to the formation of emitting plasma columns, but we assume that their existence causes regular drifting subpulses. Even if ultimately it turns out that drifting subpulses are not caused explicitly by plasma rotation, this plasma rotation should still be visible as features in the power spectrum of pulsar emission.[7]

In Section 2, we derive an expression for the angular velocity of plasma rotation relative to the NS. We point out a widespread misconception arising from the literal application of an order-of-magnitude expression for this angular velocity from Ruderman & Sutherland (1975). In that section we also argue that, using the exact expression, effects such as drift-rate variations and drift direction reversals have a natural explanation within the standard model.

In Section 3, we introduce pulsar PSR B0826−34 (hereafter B0826−34), a bright aligned rotator with subpulse drift throughout the pulse window. In Section 4, we outline the observational setup with which we measure such drift-rate variations. In Section 5, we present the relations found in Section 2 in a form that can be directly applied to such drift-rate observations,[8] and we describe the results from this fitting. We then derive the maximum variations in potential drop over the polar cap of B0826−34, effectively using the subpulse drift in B0826−34 as a voltmeter. The discussion and interpretations of these results take place in Section 6. We summarize and conclude in Section 7.

2. PLASMA ROTATION AND DRIFTING SUBPULSES

2.1. Plasma Rotation in the Open Magnetic Field Line Zone

Let us do a more careful derivation of the formula for the drift speed of plasma above the accelerating gap in the pulsar polar cap than that presented in Ruderman & Sutherland (1975). In the reference frame corotating with the NS, Faraday's law for electric and magnetic field as measured in the corotating frame has the same form as in the laboratory frame (Schiff 1939), namely,

$$\nabla \times \mathbf{E} = \frac{1}{c}\frac{\partial \mathbf{B}}{\partial t}\,. \tag{1}$$

The electric field in Equation (1) represents the non-corotational component of the electric field—the component that forces plasma to move in the rotating frame. In the corotating frame the temporal variations of the magnetic field in the polar cap can be caused only by fluctuations of currents in the magnetosphere. Even if fluctuations of the electric current are of the order of the Goldreich–Julian current $\rho_{\rm GJ}c$, the resulting variation of the magnetic field is $\delta B/B \simeq (R_{\rm NS}/R_{\rm LC})^{3/2} \simeq 6\times10^{-6}P^{-3/2}$; here $R_{\rm NS}$ is the NS radius and $R_{\rm LC}\equiv c/\Omega$ is the light cylinder radius, $\Omega_{\rm NS}$ is the angular velocity of NS rotation, and P is pulsar period in seconds. Hence, $\nabla\times\mathbf{E}=0$ with high accuracy and circulation of the non-corotational electric field along a closed path is zero (even for an inclined rotator).

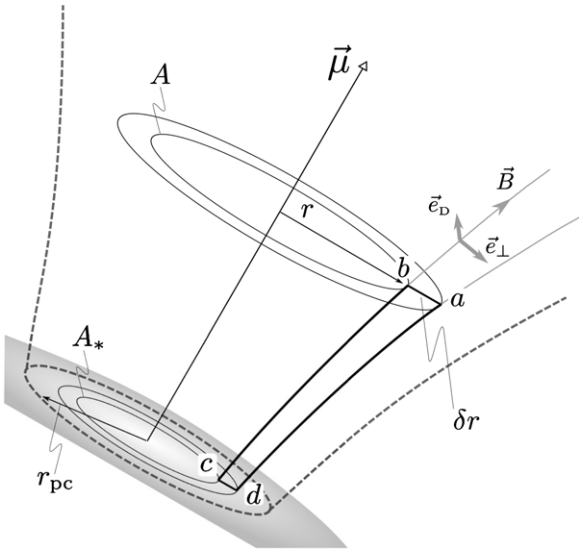

Figure 1. Schematics of the pulsar polar cap. The polar-cap boundary is shown with the dashed line. The path sections are explained in detail in the main text.

Let us consider the circulation of the electric field along a fiducial path $abcd$—see Figure 1. In the pulsar polar cap the top (ab) and bottom (cd) parts are infinitesimally small and are just below the NS surface (cd) and above the accelerating gap in the region of dense plasma with screened electric field (ab); the lateral sides (bc and da) follow magnetic field lines. Note that we consider a path that is fully in the open magnetic field line region, in contrast to the work of Ruderman & Sutherland (1975), where one lateral path was along the field line along the polar-cap boundary (see their Figure 4). To clarify our derivation, Figure 1 shows our unit vectors along positive directions for the perpendicular component of the electric field, $e_\perp$, and the drift velocity, e_D. The circulation of the electric field along this path is

$$\begin{aligned}\oint E\,dl &= -E_\perp\delta r + \int_b^c E_{||}\,dz + \int_d^a E_{||}\,dz\\ &= -E_\perp dr + V_{\rm bc} - V_{\rm ad} = 0\,,\end{aligned} \tag{2}$$

where $E_\perp$ and $E_{||}$ are components of the electric field, perpendicular and parallel to the magnetic field, respectively, while

[7] Indeed, most of the pulsars studied by Weltevrede et al. (2006, 2007) have features in the fluctuation (power) spectrum rather than clearly visible drift bands.

[8] Fitting code available at http://www.astron.nl/pulsars/papers/lt12/.

$V_{\rm bc}$, $V_{\rm ad}$ are potential drops in the accelerating gap, along magnetic field lines. $E_\perp = 0$ just below the NS surface, which we assume to be a perfect conductor. Taking the limit $\delta r \to 0$, we get for the non-corotational component of the electric field

$$E_\perp = -\frac{dV}{dr}\,. \tag{3}$$

The drift velocity of the plasma relative to the NS is then

$$v_{\rm D} = c\frac{\mathbf{E}\times\mathbf{B}}{B^2} = \frac{c}{B}\frac{dV}{dr}\,. \tag{4}$$

The drift velocity of plasma relative to the NS thus depends on the *variation* of the electric potential in the acceleration zone. For aligned pulsars this result is well-known textbook material (e.g., Beskin 2010), and for inclined rotators the correct general expression for the plasma drift velocity was explicitly mentioned in Fung et al. (2006); as we shall detail below, this result partially supersedes the Ruderman & Sutherland family of models, but it has not yet struck root. Here we want to draw special attention to it, as it has profound consequences for the interpretation of pulsar drift phenomena.

The reasoning leading up to this conclusion, i.e., the *variation* of the accelerating potential causes plasma drift, can be put differently and perhaps more insightfully: the electric field is the gradient of the electrostatic potential, $\mathbf{E} = -\nabla V$; in the co-rotating frame the potential is the accelerating potential and the perpendicular electric field $E_\perp$ is the field that causes drift relative to the NS; hence, $E_\perp = -(\nabla V)_\perp = -\partial V/\partial r$. If, for example, the potential drop is the same along all polar-cap magnetic field lines, there is no relative rotation of plasma, however large the potential drop is. In that case, though, there is a region very close to the polar-cap boundary where the potential drop plummets to zero at the last closed magnetic field line. Plasma in that region will have a very large drift velocity.

The original derivation of the expression for $v_{\rm D}$ in Ruderman & Sutherland (1975) is similar to our derivation here, but instead of expressing $v_{\rm D}$ in terms of the derivative of the accelerating potential dV/dr, an order-of-magnitude estimate is used: their Equation (31) is equivalent to our Equation (4), but using the entire potential drop along a field line V for dV and half of the polar-cap radius, $r_{\rm pc}/2$, as an estimate for dr. Yet, the potential drop in the pair-production zone is expected not to vary much from one field line to another, except at the boundaries of the active zone (e.g., Harding & Muslimov 1998; Hibschman & Arons 2001); the active zone is also expected to be a noticeable part of the polar cap, at least in the space charge limited flow model (Arons & Scharlemann 1979). Hence, the Ruderman & Sutherland (1975) order-of-magnitude prediction for the drift rate is a large overestimate. And indeed, the drift-rate speeds predicted by Ruderman & Sutherland (1975) in their Equation (31) are much larger than those observed—for example, the very slow but steady drift rate observed in PSR B0809+74 (van Leeuwen et al. 2003) is incompatible with this order-of-magnitude estimate. Thus, in the most detailed drifting-subpulse models based on Ruderman & Sutherland (1975), a substantial reduction of the accelerating potential is necessary to reproduce these observed slow drift rates. In Gil & Sendyk (2000) and Gil et al. (2003), this is achieved by assuming highly non-dipolar polar-cap magnetic fields and by fine-tuning the particle flux impact to produce the critical surface temperature.

Furthermore, literal application of Ruderman & Sutherland's (1975) expression for the plasma drift speed (i.e., in the form $v_{\rm D} = cV/r_{\rm pc}B$) has difficulty explaining the drift-rate variations with time or longitude that are observed in several pulsars (such as the bidirectional drift bands in PSR J0815+09; Champion et al. 2005) and is incapable of producing the complete drift direction reversals seen in PSR B0826−34. The explanation for such observed subpulse-drift reversals usually involves aliasing. In the case of B0826−34 this requires the circulation frequency to be fine-tuned to the rotation frequency, such that the aliased subpulses appear to move only very slowly; and indeed Gupta et al. (2004) were able to construct such a model. However, Esamdin et al. (2005) find that the observed reversals influence the intrinsic subpulse brightness, strongly suggesting that the reversal is not just apparent, but actually occurs in the corotating frame. The existence of such real reversals thus suggests a failing of the $\mathbf{E}\times\mathbf{B}$ family of models.

We want to point out that all these apparent discrepancies between model and observation are non-existent. Using the derivation we present here, in Equation (4), no fine-tuning or additional assumptions, such as strong higher-order magnetic fields, are needed to explain the observed subpulse-drift properties. The drift rate depends on the variation of the potential drop from one field line to another. The potential drop can be very large, but if it does not change much across the polar cap, the drift rate will be slow. Depending on whether the potential drop increases or decreases toward the center of the polar cap, the drift rate will be in one or another direction. If the potential-drop derivative at the line of sight varies with time, the observed drift speed changes and can even reverse. In Section 5, we use subpulse-drift data from B0826−34 to show that the variation of the accelerating potential necessary to explain these phenomena is small indeed and that the model is plausible.

We reiterate that we are not solving these problems by introducing extra assumptions on how the potential drop varies. Equation (4) simply *is* the correct dependence for the drift velocity of the plasma; it is not a fine-tuning or modification of the previously widely used order-of-magnitude expression for $v_{\rm D}$. If drifting subpulses are indeed due to plasma motion relative to the NS, all their properties depend on the variation of the potential drop and not on the potential drop itself. In Section 6, we will also argue that all the properties of the accelerating potential necessary for explanation of various properties of drifting subpulses seem to be integral properties of the standard pulsar model.

2.2. Connecting with Observations of Drifting Subpulses

In pulsars with subpulse drift, Equation (4) can be used to set limits on the local parameters of the pulsar polar cap. There, a measurement of the plasma drift velocity provides the value of the radial derivative of accelerating potential. In practice, however, the quantity that subpulse-drift observations produce is the angular drift velocity of subpulses within the pulsar profile, not the plasma drift velocity in the pulsar coordinate frame that is needed in Equation (4). Below we derive expressions that connect observable parameters to the variation of the accelerating potential.

The momentary angular velocity of plasma relative to a magnetic axis is

$$\Omega_{\rm D} = \frac{c}{Br}\frac{dV}{dr}\,, \tag{5}$$

where r is the distance between our sight-line path and the magnetic axis. When we derived this expression in Section 2.1, we considered the path segment ab in the region above the

accelerating gap where electric field is screened, and so B, r, dr in Equation (5) are also taken in some plane perpendicular to the magnetic axis $\boldsymbol{\mu}$, in the region with screened electric field (see Figure 1).

Our path $abcd$ has lateral sides that follow magnetic field lines; hence, if Φ is the magnetic flux limited by some closed path passing through our fiducial point (e.g., the path A or A_* in Figure 1), then $Br = \partial\Phi/\partial r\partial\varphi$, where φ is the azimuthal angle. For any magnetic field that is axisymmetric relative to some magnetic axis, the plasma drift relative to the NS will be a rotation around this magnetic axis. The magnetic flux can be measured as the flux through a circle of radius r, and Equation (5) takes the form

$$\Omega_{\rm D} = 2\pi c \frac{dV}{d\Phi}. \tag{6}$$

It will be convenient to normalize the potential drop along a magnetic field line to the potential drop across magnetic field lines at the NS surface between the rotation axis and the boundary of the polar cap in an aligned pulsar with the same period:

$$\Delta V_{\rm vac} = -\int_0^{r_{\rm pc}} E\, dr = \frac{1}{2}\frac{\Omega_{\rm NS}}{c} B r_{\rm pc}^2 = \frac{\Omega_{\rm NS}\Phi_{\rm pc}}{2\pi c}$$
$$\simeq 6.6\times 10^{12} R_{\rm NS,6}^3 B_{12} P^{-2}\ {\rm V}, \tag{7}$$

where $r_{\rm pc}$ is the polar-cap radius, $\Phi_{\rm pc}$ is the magnetic flux through the polar cap, B_{12} is the magnetic field strength in units of 10^{12} G, and $R_{\rm NS,6}$ is the NS radius in 10^6 cm. In doing this numerical estimate, we assumed that the polar cap is small enough that the variation of the magnetic field over it is negligible. $\Delta V_{\rm vac}$ is a good estimate for the available potential drop—if there were vacuum in the open magnetic field line zone, the potential drop along magnetic field lines in the polar cap would reach a value comparable to $\Delta V_{\rm vac}$ at the height $\sim r_{\rm pc}$ from the NS surface and then vary very slowly with the altitude, approaching its maximum value $\Delta V_{\rm vac}$ from below.

Normalizing the magnetic flux to $\Phi_{\rm pc}$, we get from Equation (6)

$$\frac{\Omega_{\rm D}}{\Omega_{\rm NS}} = \frac{d\tilde{V}}{d\tilde{\Phi}}, \tag{8}$$

where $\tilde{V} \equiv V/\Delta V_{\rm vac}$ and $\tilde{\Phi} \equiv \Phi/\Phi_{\rm pc}$. The normalized magnetic flux is $\tilde{\Phi} = (r/r_{\rm pc})^2 = (\theta/\theta_{\rm pc})^2$, where θ is the colatitude measured from the magnetic axis. Let us denote the colatitude to the colatitude of the polar-cap boundary as

$$\xi \equiv \frac{\theta}{\theta_{\rm pc}}; \tag{9}$$

then in terms of ξ, Equation (8) takes the form

$$\frac{\Omega_{\rm D}}{\Omega_{\rm NS}} = \frac{1}{2\xi}\frac{d\tilde{V}}{d\xi}. \tag{10}$$

After one rotation the difference in phase between a fiducial point at the NS surface and an emitting column will be

$$\delta\phi_1 = \Omega_{\rm D} P = \frac{\omega_{\rm D}\pi}{180^\circ}, \tag{11}$$

where $\omega_{\rm D}$ is the drift velocity in units of degrees/period. Using Equation (10), we can then write the derivative of the accelerating potential as (hereafter we use V instead of $\tilde{V}$)

$$\frac{dV}{d\xi} = \xi\frac{\omega_{\rm D}}{180^\circ}. \tag{12}$$

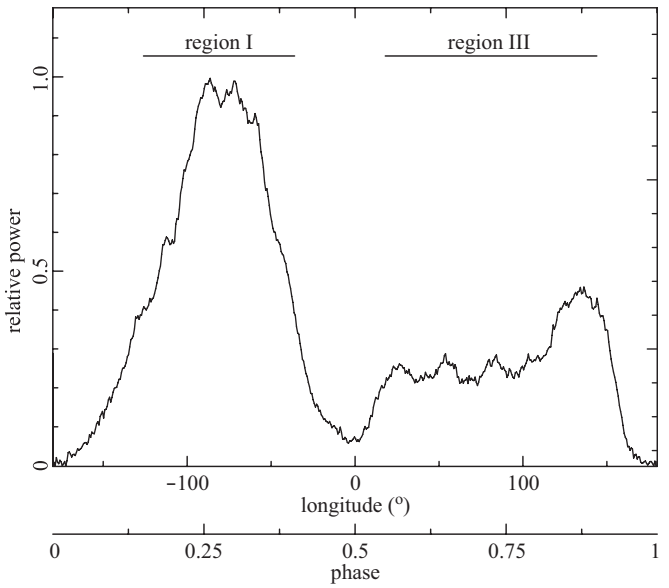

Figure 2. 360° average profile of B0826−34 in the strong mode. 1500 s of data from observation PT0168_116 were integrated.

Thus, if we measure the angular velocity at one colatitude, we can now calculate the derivative of the accelerating potential at that point. If we could measure it at two different colatitudes, we can set limits on the accelerating potential, assuming a gradual variation of the potential across the polar cap. For such a study our line of sight must cross two separate drift bands at different colatitudes. An ideal case would be a bright, slightly inclined rotator where the line of sight crosses two regions at different colatitudes, each for a significant fraction of period such that any drifting subpulses are clearly visible; B0826−34 is such a pulsar. It has two separate drift bands that are thought to represent emission from different colatitudes. This pulsar provides us a unique opportunity to put direct observational constraints on the physical conditions in the polar-cap accelerating zone—the heart of the pulsar.

3. PSR B0826−34

Pulsar B0826−34 was discovered as a broad profile but very intermittent pulsar (Manchester et al. 1978). Figure 2 shows how the pulse profile basically spans 360°. B0826−34 emits strongly only 30% of the time. When not in this strong mode, no emission could be detected and the pulsar appeared to be in a "null" state (Durdin et al. 1979). Several years after these first studies at 408 and 635 MHz respectively, Esamdin et al. (2005) revisited B0826−34 with new Parkes data at 1.4 GHz and found that during the null state a weak, different pulse profile is emitted (see Figure 4). In 2008, Bhattacharyya et al. (2008) did not detect a weak-mode profile in GMRT data at six frequencies between 157 and 1060 MHz; yet Parkes observations at 685 and 3094 MHz confirm the existence of this weak-mode emission (Serylak 2011).

Soon after the initial discovery, B0826−34 was found to display drifting subpulses over more than half of its pulse period. At times, up to nine drift tracks are visible. Most remarkable is the occasional reversal of drift direction (Biggs et al. 1985).

The combination seen in B0826−34, of a broad profile that cuts through different lines of sight from the magnetic pole and a system of highly varying drifting subpulses, is unique. The number of pulsars that show some kind of periodic modulation is

Table 1
Details of the Four Observing Sessions Used in This Paper

OBSID	t (hr)	Date (MJD)	t_{samp} (ms)	Strong Mode (s)
PT0168_116	6	52527	1.0	1939−3535
PT0168_150	6	52528	1.0	(none)
PT0169_106	4	52579	0.25	0−7221
PT0169_152	4	52580	0.25	(none)

Notes. Observation identifier OBSID, duration t, date, and sampling time t_{samp} are shown. The last column marks the begin and end times of any strong mode sections in the data, indicated in seconds since the start of the observation.

substantial (>50%; see Weltevrede et al. 2006 for an overview), and most of those show drift-rate variations with time and/or pulse longitude. But there are only a handful, at most, of bright wide-profile or nearly aligned rotators like B0826−34 known (e.g., B0818−41; Bhattacharyya et al. 2007). And although some pulsars, such as PSR B2303+30 (Redman et al. 2005), have different modes in which drift rates appear to be in opposite directions, B0826−34 is the only source in which the intrinsic drift rate gradually reverses outright (Esamdin et al. 2005).

4. OBSERVATIONS AND DATA REDUCTION

Pulsar B0826−34 was observed for a total of 20 hr on 2002 September 10 and 11 and November 1 and 2. The middle beam of the multibeam receiver on the Parkes telescope was used, at a central observing frequency of 1372 MHz. A 288 MHz wide observing band was split over 96 × 3 MHz channels in the analog filter bank (Manchester et al. 2001). The total power from each of the filter channels was recorded every 0.25/1.0 ms (Table 1).

These filter bank data were retrieved from the `PT_TAPES` section of the Australian Pulsar Timing Archive,[9] for projects `P276` and `P417`. They were unpacked using `sc_td` and converted from the original 1 bit to the more standard 8 bit filterbank format for compatibility.[10] We next inspected each of the four observations with PRESTO[11] to remove radio interference. Starting from the known ephemeris (Hobbs et al. 2004) and the dispersion measure of 52 pc cm^{-3} (Bhattacharyya et al. 2008), the data were folded and dedispersed at the period, period derivative, and dispersion measure that maximized signal-to-noise ratio.

4.1. Identifying Mode Changes and Nulls

Using fitSubPulses (van Leeuwen et al. 2002), we next automatically and visually inspected the data for nulls and mode changes. These are robustly separated in a pulse-energy histogram (Janssen & van Leeuwen 2004) and verified manually. In Figure 3 we show several nulls and a transition from strong to weak mode. In two of the four sessions, `PT0168_150` and `PT0169_152` (Table 1), the pulsar emitted in the weak mode for the entire session. In the two other observations strong-mode sequences are found, one of ∼2000 and one of ∼7000 s duration (i.e., ∼1000 and ∼4000 individual pulses for this 1.85 s period pulsar). In Figure 4, we show the long-term behavior in the strong and weak mode and a transition between the two.

[9] http://www.atnf.csiro.au/research/pulsar/archive/
[10] http://sigproc.sourceforge.net/
[11] http://www.cv.nrao.edu/∼sransom/presto/

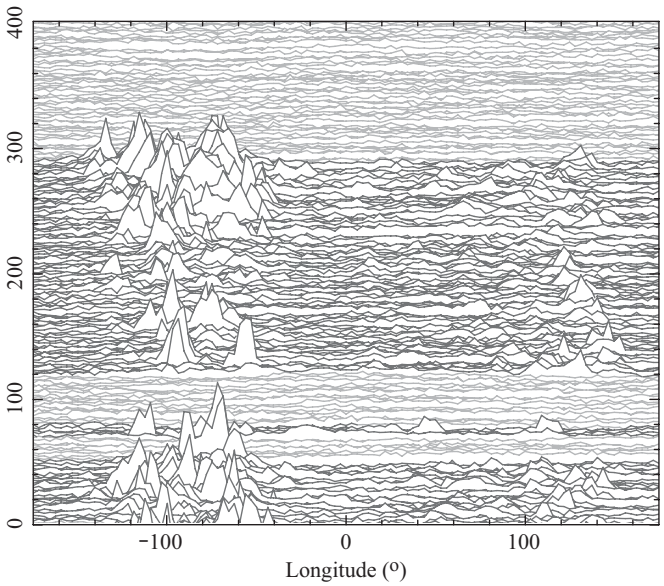

Figure 3. Pulse stack with several nulls in light gray and a transition to a weak-mode interval lasting several thousand pulses, starting at pulse number 300. For both the nulls and the mode transition, there is a clear separation between on and off pulses in the pulse-energy histogram.

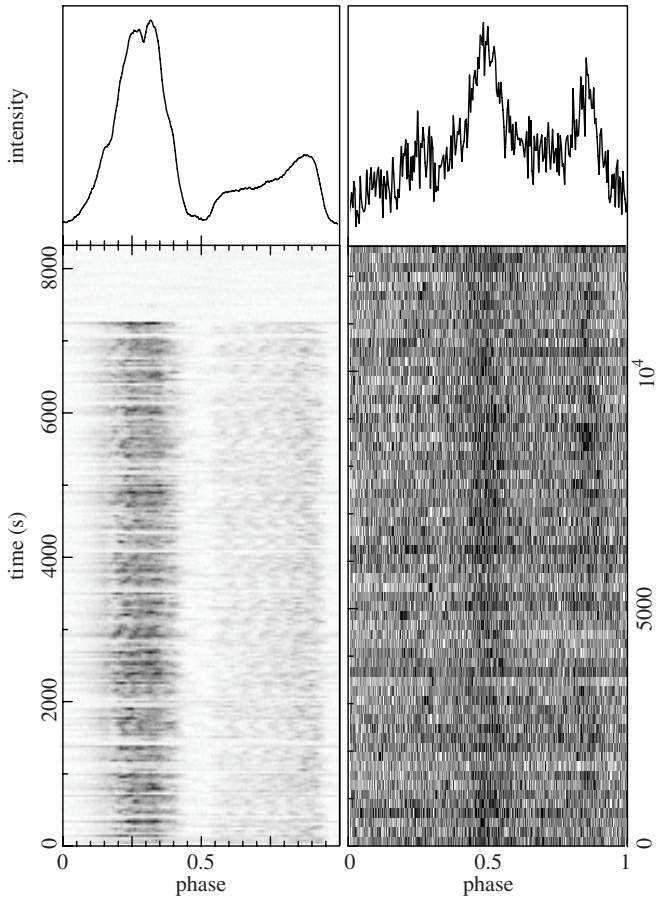

Figure 4. Plots of intensity in gray scale vs. phase and time (bottom panels) and of the integrated profiles over the entire observation (top panels). The intensity in the top panels is in arbitrary units, and the two observations are not plotted to scale. A 2 hr strong-mode sequence from the start of observation PT0169_106 is shown on the left, and a 4 hr weak-mode observation is shown on the right (PT0169_152).

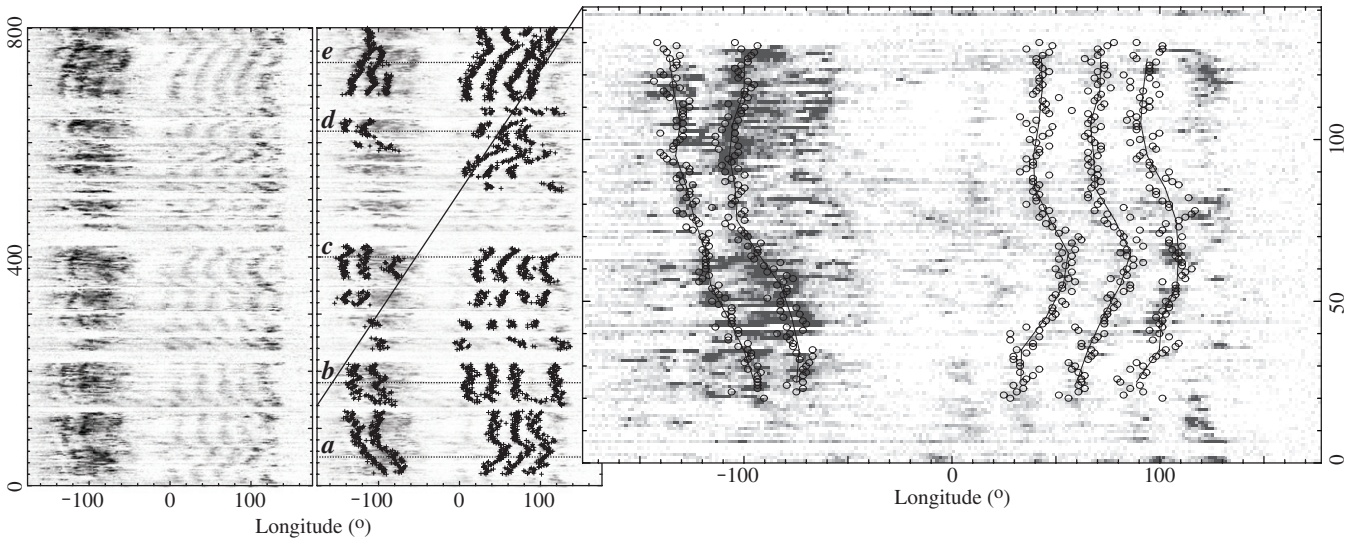

Figure 5. Strong-mode sequence about 800 pulses long from observation PT0168_116 (left), the results of fitting for the locations of the subpulses (middle), and the final fits to drift tracks for the initial ∼100 pulses (right). Up to five or six drift bands are usually identified. In the middle and right plot, the contrast of the pulse stack was halved to make the fit markers more visible. For the dotted lines labeled *a*–*e* in the middle panel the potential drop is derived and plotted in Figure 9.

4.2. Determining Drift Rates

Within the strong-mode sequences, we next worked toward identifying drift rates and directions. Our aim was to characterize the variations in subpulse drifting over the wide profile. We thus fit for the location of individual subpulses. This is in contrast to the method described by Esamdin et al. (2005) for B0826−34, where a comb-like template with nine main drift tracks at fixed spacings was used to come to an estimate of the drift rate averaged over all drift tracks. Such a method cannot measure drift rates that vary with pulse longitude, as is seen in many pulsars (Weltevrede et al. 2006). For each strong-mode pulse, we thus fitted for the location of individual subpulses: we smoothed the single-pulse profile by a 4 ms window (the approximate average width of the subpulses) and then determined the location of the maximum. The maximums in subsequent single pulses were next grouped together, if they were less than half the average subpulse separation apart in phase. Only tracks with more than 10 subpulses were retained. In this manner, subpulse tracks of more than 100 pulses were robustly identified. Within each of these tracks, the variation in drift speed and direction was next measured by least-squares fitting to subsequent sets of 10 subpulses, as illustrated in the rightmost panel of Figure 5.

5. MODELING

In the strong mode, B0826−34 emits mainly in two regions. In Figures 2 and 4 these are the brighter phase range 0.15–0.40 and the dimmer range 0.55–0.9. Esamdin et al. (2005) label these regions I and III, respectively. They find that in region I both the width and separation of the subpulses are reduced by a factor of 1.22 compared to region III, from which they conclude that region I is closer to the magnetic axis than region III.

We now use the drift speeds in these two regions to model the variation of the acceleration potential in B0826−34. We define band 1 as the band near the edge of the polar cap, i.e., the region empirically numbered III, and band 2 as being the closest to the magnetic axis, i.e., region I (the leftmost band in Figure 4). The drift speeds and colatitudes of band 1 and 2 are $\omega_{\mathrm{D},1,2}$ and $\xi_{1,2}$. We know the separation between these drift bands $\Delta\xi \simeq 0.2$ and assume that band 1 is near the edge of

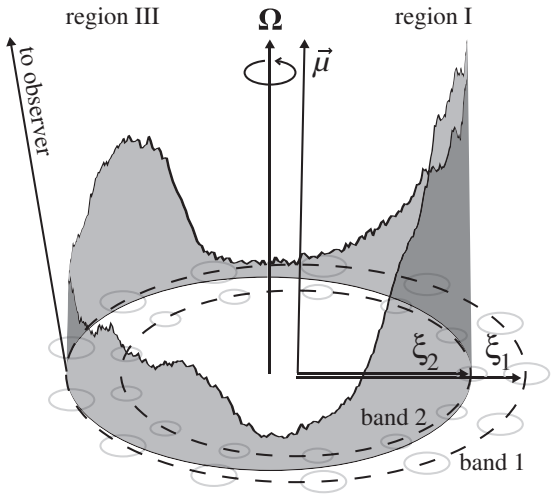

Figure 6. Diagram of the geometry used in this paper, for the polar-cap region of B0826−34. Folded on the line of sight to the observer is the 360° pulse profile from Figure 2. Regions I and III from that figure are also indicated. The angles between rotation axis $\boldsymbol{\Omega}$, the magnetic axis $\boldsymbol{\mu}$, and the line-of-sight angle to the observer are from Esamdin et al. (2005); the system of two rings of subpulses, one realization of which is illustrated on the bottom plane, is after Figure 10 in that same paper. The colatitudes of our bands 1 and 2 are marked $\xi_{1,2}$.

the polar cap, so $\xi_1 \simeq 1.0$ (Esamdin et al. 2005). In Figure 6, the observed strong-mode profile from Figure 2 is shown in this geometry. We have freedom for setting V at ξ_1 to an arbitrary value; let it be zero—we have an equation only for $dV/d\xi$. We thus have three known parameters, $(dV/d\xi)_{1,2}$ and $V(\xi_1) = 0$, such that we can fit for $V(\xi)$ with a parabola:

$$V(\xi) = a\left(\xi^2 - \xi_1^2\right) + b(\xi - \xi_1)\,. \tag{13}$$

Using this parabolic fit, we next derive the maximum potential drop that our line of sight comes across in B0826−34. The values of the coefficients are determined from Equation (12) at points ξ_1, ξ_2. Depending on the values of these coefficients, $V(\xi)$ either has a local extremum at the point $\xi_{\mathrm{ex}} \in [\xi_2, \xi_1]$ or is a monotonic function of ξ. The position of the extremum

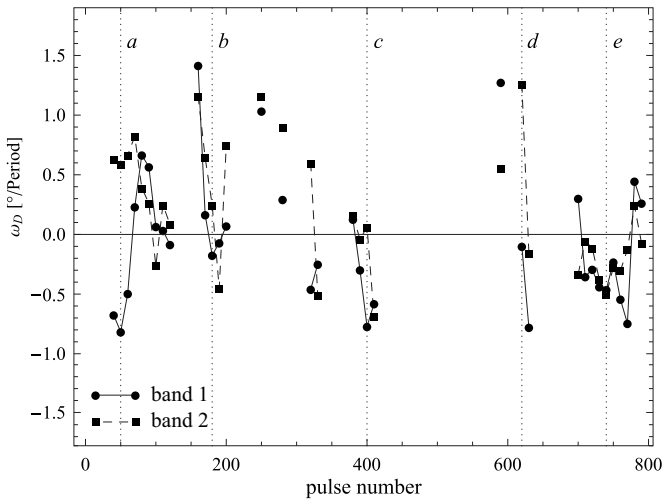

Figure 7. Drift speed ω_D (degrees per period) in two bands as functions of pulse number. The drift speed for band 1 is shown by filled circles connected by a solid line, for band 2 by filled squares connected by a dashed line. Dotted lines labeled *a*–*e* show pulses for which we plot the potential drop in Figure 9.

is $\xi_{ex} = -b/2a$, and if it is inside the interval $[\xi_2, \xi_1]$, the maximum potential drop variation ΔV^{ex}_{max} between points 1 and 2 is either $V(\xi_{ex})$ or $V(\xi_{ex}) - V(\xi_2)$, depending on which absolute value is larger. The general expression for the maximum potential drop variation in colatitude interval $[\xi_2, \xi_1]$ is then

$$\Delta V_{max} = \begin{cases} \Delta V^{ex}_{max}, & \text{if} \xi_{ex} \in [\xi_2, \xi_1] \\ V(\xi_2), & \text{if} \xi_{ex} \notin [\xi_2, \xi_1]. \end{cases} \quad (14)$$

To each of the drift tracks identified in data set PT0168_116, line segments of 10 pulses were fitted, as shown in Figure 5. The slope of these segments is the drift velocity ω_D, where we define positive ω_D as drifting toward earlier arrival. For band 1, the drift rate of up to three tracks was averaged to obtain $\omega_{D,1}$; for band 2, $\omega_{D,2}$ is the average of up to two drift tracks (see Figure 5). The resulting drift speeds range from $-1.^\circ0$ to $+1.^\circ5$ per period and are plotted in Figure 7. Figures 5 and 7 show that while bands 1 and 2 generally show the same drift rate, as assumed for data reduction in Esamdin et al. (2005), there are several periods in which the drift rate between the bands is significantly different.

For all sections with drift-rate estimates, the maximum potential drop difference ΔV_{max} was next derived using Equations (12)–(14). The resulting potential drop variations, plotted in Figure 8, are of order of several $10^{-4}\, V_{vac}$. In Figure 9, the fitted shape of the potential drop is shown for five representative sections labeled (a–e) in Figure 5.

The potential drop variations shown in Figures 8 and 9 assume that our outer sight line traverse is close to the edge of the polar cap, i.e., $\xi_1 \simeq 1.0$. If the actual geometry is described with a smaller value for ξ_1, the reported potential drop values scale down linearly.

A Mathematica notebook containing these equations as well as routines to derive potential drop curves from drift-rate data is publicly available.[12]

So, from Figures 8 and 9 it follows that the accelerating potential varies in both space and time. The spatial variations occur between the two drift bands, over a range as large as 20% of the polar-cap radius; the temporal variations occur on

[12] http://www.astron.nl/pulsars/papers/lt12/

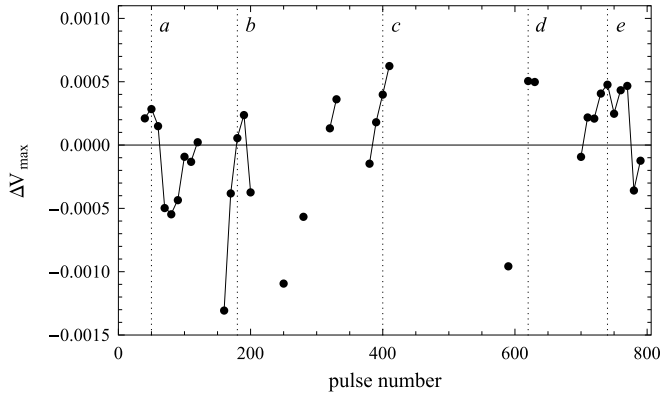

Figure 8. Maximum potential drop difference per Equation (14) in the colatitude interval between the two drift bands, as a function of pulse number. ΔV_{max} is normalized to the vacuum potential drop. Notations are the same as in Figure 7.

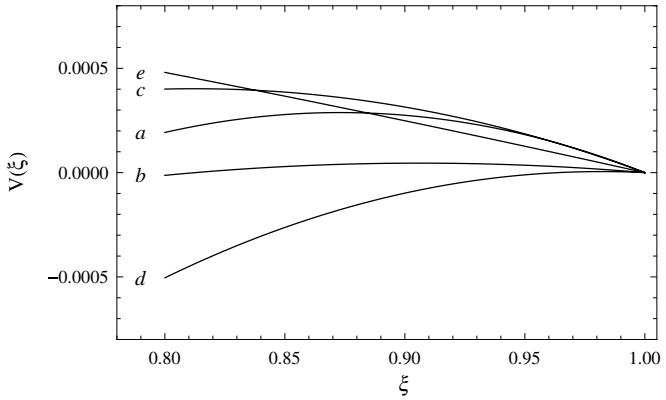

Figure 9. Potential drop variation according to Equation (13) in the colatitude interval between the two drift bands, for pulses marked by *a*–*e* in Figures 7 and 8, as a function of the normalized colatitude $\xi \equiv \theta/\theta_{pc}$. $V(\xi)$ is normalized to the vacuum potential drop.

timescales much larger than pulsar rotation period. Still, both types of variations are very small—of order only several times $10^{-4}\, \Delta V_{vac}$.

If we next derive the nominal vacuum potential drop for B0826−34 per Equation (7), using $R_{NS,6} = 1.0$, $B_{12} = 1.4$, and $P = 1.85$, we find $\Delta V_{vac} = 2.7 \times 10^{12}$ V. Thus, using pulsar B0826−34 as a voltmeter indicates that the variations in its acceleration potential are of the order of only 10^9 V.

6. DISCUSSION

Below we propose a qualitative model for drifting subpulses and discuss potential future work.

6.1. A Model for Drifting Subpulses

The accelerating potential estimates we produce only make the general assumption that subpulses are produced by emitting features that are stationary relative to the outflowing plasma in the polar-cap region, and their drift is due to the rotation of this plasma, relative to the pulsar. Here we wish to propose a more specific, but still qualitative and schematic, model for drifting subpulses that well fits the de facto standard force-free model of pulsar magnetospheres and that is consistent with the results presented in this paper.

6.1.1. Timescales

First, we address the question why drift rates can change on timescales much larger than the pulsar's rotational period. In the frame of the force-free pulsar model, the potential drop in the pulsar polar cap depends on the current density flowing along a given magnetic field line and not only on the local physics of the polar cap (e.g., Levinson et al. 2005; Timokhin 2006; Beloborodov 2008; Timokhin 2010b). Yet this current density depends on the *global* magnetospheric configuration (e.g., Timokhin 2007c, 2007a, 2007b; Bai & Spitkovsky 2010; Li et al. 2012; Kalapotharakos et al. 2012). Changes in the accelerating potential in the polar cap should be, therefore, manifestations of changes in the global magnetosphere configuration. At some stages of the pulsar spin-down evolution, Timokhin (2010a) suggested, this pulsar magnetosphere can change its configuration on timescales much larger than the pulsar period and/or have meta-stable states. In the standard model, the pulsar magnetosphere, the polar-cap cascade zone, and the current sheet zone carrying most of the return current are tightly coupled. As these regions all have different timescales, the resulting system might constitute a highly nonlinear dynamical system with varied behavior on a wide range of characteristic timescales (Timokhin 2010a). Hence, the pulsar magnetosphere as a whole determines the properties of pulsar emission; such an idea in general was discussed before by Wright (2003), for example.

So, when the global configuration of the magnetosphere changes, the current density distribution and the accelerating potential in the polar cap change with it, as does the plasma drift velocity in the open field-line zone. Nonlinear dynamical systems can evolve on very long timescales, and so the pulsar magnetosphere might also change on timescales much larger than that of its composing parts. The pulsar under study here, B0826−34, is not unique in exhibiting changes on timescales many times larger than the rotation period: after some mode switches, pulsar B0943+10, for example, shows a gradual drift-speed change on a 4000-period timescale (Rankin & Suleymanova 2006). Conversely, if a magnetosphere switches between meta-stable configurations, this results in mode changing and/or nulling. Because these configurations have different current density distributions, we claim that with any mode change, the subpulse-drift rate must change too. Several mode-changing pulsars are already known to exhibit such markedly different subpulse drift in different modes (e.g., PSR B0031−07, Smits et al. 2005; PSR B1944+17, Kloumann & Rankin 2010).

6.1.2. Magnitude of Potential Drop Variations

Given the accelerating potential in B0826−34, we next discuss how large the inferred variations are, compared to its absolute value. The maximum achievable voltage in the polar cap is of the order of the potential drop across it; the vacuum potential drop $\Delta V_{\rm vac}$ in our terminology. At some point the onset of pair creation screens the electric field and limits the extent of the accelerating zone. Especially in young pulsars the height of the acceleration zone is much smaller than the width of the polar cap, and the potential drop is much less than the corresponding $\Delta V_{\rm vac}$.

Now, recent self-consistent simulations of pair cascades in the polar cap (Timokhin 2010b; A. N. Timokhin & J. Arons 2012, in preparation) have shown that this pair-plasma generation is non-stationary, i.e., that each period of particle acceleration is followed by a quiet phase, in which the accelerating electric field is screened and no pairs are produced. This holds for both the Ruderman & Sutherland (1975) and space charge limited flow (Arons & Scharlemann 1979) regimes. In these simulations, the cascade behavior depends on the current density: that density defines the duration of the active and quiet phases; it also determines the maximum potential drop in the active phase. Thus, these simulations strongly suggest that traditional estimates for the potential drop (e.g., Ruderman & Sutherland 1975; Hibschman & Arons 2001) are very inaccurate.

The source under study in this paper, B0826−34, is a rather long-period pulsar, with $P = 1.85$ s, located close to the pulsar death line. If we assume that the cessation of pair plasma production is responsible for a pulsar's demise, then the potential drop in B0826−34 should be close to its maximum possible value: the vacuum drop. In Section 5, we found potential-drop variations with time of $<10^{-3}\Delta V_{\rm vac}$, i.e., very small compared to the value of the potential drop, even if the actual potential drop would be an order of magnitude smaller than the vacuum drop.[13]

The magnetospheric configuration changes that cause such one-in-a-thousand acceleration-drop fluctuations should be very small and are unlikely to influence the stability of the magnetosphere or be visible in profile or spin-down-rate variations. Overall, to us the inferred small magnetospheric fluctuations seem quite plausible.

6.1.3. Plasma and Drifting Subpulses

Finally, let us now address the question of what could cause these stationary features in the outflowing electron–positron plasma that manifest themselves as drifting subpulses. The current most standard explanation (Ruderman & Sutherland 1975) assumes that plasma generation in the pulsar polar cap occurs in "spark columns" that are isolated by vacuum and that these columns drift relative to the NS. The plasma then flows only along certain magnetic field lines, and thus the emitting regions are spatially localized. In our view, such a picture has serious difficulties. We will outline these below.

First, because of the magnetic field line curvature, any spark column should quickly drift toward the magnetic pole, as pair-plasma generation with each cascade iteration occurs closer to the magnetic symmetry axis. Gil & Sendyk (2000) have suggested that in a specific symmetric configuration with a central spark, a polar cap stably packed with sparks could exist. More detailed simulations are necessary to prove that this could indeed be the case even in such a symmetric configuration. Recent self-consistent simulation of pair cascades (Timokhin 2010b) has shown that the characteristic timescale between discharges can be much larger than previously assumed. This indicates that the electrodynamics of the cascade zone, even for short-period pulsars, resembles more strongly a long tube with conducting walls than a short cylinder with all characteristic dimensions of order the polar-cap width $r_{\rm pc}$ (as assumed in Ruderman & Sutherland 1975 models). This would imply that the coupling of the accelerating electric fields across the polar is more complex than assumed before, calling into question the existence of distinct quasi-stable spark patterns such as those proposed in Gil & Sendyk (2000).

[13] Traditional estimates for the potential drop for B0826−34, for dipolar and strongly non-dipolar (magnetic field-line curvature of 10^6 cm) fields, respectively, are $\sim\Delta V_{\rm vac}$ and $0.03\Delta V_{\rm vac}$ for the space charge limited flow (using expressions from Hibschman & Arons 2001). For the Ruderman & Sutherland (1975) model we get $0.6\Delta V_{\rm vac}$ and $0.04\Delta V_{\rm vac}$.

Second, we have thus far used Equation (4) on a polar cap that is completely filled with plasma; the equation is, however, equally applicable to plasma columns surrounded by vacuum. Outside of the plasma column the electric field is unscreened, and the accelerating potential along the magnetic field lines there is much higher than inside the column, where the accelerating electric field is (partially) screened by the pair plasma. Now the shape and variation of the potential drop *inside* the plasma column determine the plasma drift velocity. Magnetospheric parameters like the magnetic field strength or the current density should not change much over the width of the column. The column is much smaller than the polar cap, and column properties are set by the local physics such as the local plasma density. The magnetic field line in the plasma column that has the maximum plasma density (the column "center") should then have the smallest potential drop. Thus, V reaches its minimum value here, and the plasma *does not drift* there. The potential drop rises from this minimum value toward all column edges. Plasma on opposite sides of the column "center" will drift in opposite directions; a symmetric plasma column, for example, on average does not drift at all, which is striking. This invariably raises the question of spark-column stability, as such differential rotation leads to azimuthal smearing of the spark column. Of course, our arguments rely on a rather qualitative picture for the plasma column, and only accurate multidimensional simulations of pair cascades can verify them, but they are nevertheless more rigorous than the original Ruderman & Sutherland (1975) argumentation.

Based on these arguments, we speculate that, in time-average sense, in the active zone of the polar cap, pair productions happen uniformly, without vacuum regions along some magnetic field lines. The potential-drop variation across the active zone is therefore rather small, and so the plasma drift is slow. The distinct emitting features in such plasma flow could be due to current filaments, somewhat similar to ones observed in auroras. If so, the generation of a quasi-stationary system of such filaments depends on the global magnetosphere structure, which could then also explain its longevity.

Formation of a stable filament pattern may require a specific magnetosphere configuration, thus happening in only some pulsars. For pulsars where stable filament structures cannot form (i.e., where filaments form and disappear chaotically), there will be no clearly visible drifting subpulses. In those pulsars, however, steady plasma rotation still occurs. And indeed, most of the pulsars studied by Weltevrede et al. (2006, 2007) that do not show clear, stable drift bands still have periodic features in their power spectra—in our interpretation manifestations of the underlying *plasma rotation*.

6.2. Future Work

Certain observations could verify or falsify our model.

In this paper, we relied on the geometrical model of B0826−34 proposed by Esamdin et al. (2005). Only with a more accurate geometrical model can we place more robust constraints on the plasma rotation in the polar cap on this pulsar. Polarization measurements can constrain this emission geometry by measuring the polarization angle sweep. Such observations would have to be undertaken with sufficient collecting area, as only single-pulse polarization measurements can identify and correct for the orthogonal mode changes in B0826−34 (Lyne & Manchester 1988).

Using their averaging technique, Esamdin et al. (2005) followed the strong drift tracks and integrated all single pulses that have the same drift track phase. Those average profiles suggest that drift tracks exist in between the two strongly emitting regions. These tracks sample co-latitudes between our two extremes $\xi_{1,2}$. Observations with higher sensitivity than those presented here could measure the pulse-to-pulse drift-rate changes of those weak subpulses and provide an acceleration potential estimate over the intermediate range of colatitudes.

If observations at higher frequencies sample lower emission heights (Cordes 1978), where the polar-cap radius $r_{\rm pc}$ is reduced, then the observer sight line may start to cross $r_{\rm pc}$. From that, the extent of the polar cap and the values of $\xi_{1,2}$ could be derived. In recent observations at 3094 MHz (Serylak 2011) the pulse profile of B0826−34 still spans 360°, however, so any evidence for a decreasing pulse width would have to be sought at even higher frequencies.

After the report of the existence of the weak emission mode in B0826−34 by Esamdin et al. (2005), no evidence for such a mode was found by Bhattacharyya et al. (2008), down to an upper limit reported to be more constraining than the original detection in Esamdin et al. (2005). In addition to the confirmation of the weak mode at 685 and 3094 MHz in (Serylak 2011), we have here detected B0826−34 in weak mode in all data sets from Table 1, including in the data not originally used by Esamdin et al. (2005), such as the data set in the right panel of Figure 4.

In the model we suggest, the weak mode is a magnetospheric state that is different from the strong mode and should have a different plasma drift rate. Thus, the detection of subpulse drift in the weak mode would provide a stringent test of the general model we propose.

7. CONCLUSIONS

In this paper, we pointed out that plasma rotation in the open magnetic field-line zone depends not on the value but on the *variation* of the accelerating potential across the polar cap. If drifting subpulses are caused by this plasma drift, then by measuring the drift rate at two different colatitudes one can set limits on the accelerating potential variation between these colatitudes. We next applied this technique to observations of aligned rotator B0826−34, a favorably oriented but otherwise average regular pulsar. Thus, the limits on the potential drop variation we obtained are representative for ∼1 s pulsars.

We found that the accelerating potential varies over the colatitude range $\sim 0.2\theta_{\rm pc}$ by a factor of only several times 10^{-4} of the vacuum potential drop over the polar cap. In B0826−34, drift rates change with time, suggesting that the accelerating potential along a given magnetic field line changes with time as well. The temporal variations of the potential drop are again a few times 10^{-4} of the vacuum potential over the polar cap, of the same order as the potential difference across the colatitude range of the drift bands.

The smallness of these variations points to a remarkable stability of the potential drop over these colatitudes and provides useful constraints on (future) self-consistent models of plasma generation in pulsars.

We thank Jonathan Arons for helpful discussions. J.v.L. was supported by the European Commission (grant FP7-PEOPLE-2007-4-3-IRG #224838). A.T. was supported by an appointment to the NASA Postdoctoral program at NASA/Goddard Space Flight Center, administered by ORAU and also by NSF grant AST-0507813; NASA grants NNG06GJI08G, NNX09AU05G; and DOE grant DE-FC02-06ER41453.

REFERENCES

Arons, J., & Scharlemann, E. T. 1979, ApJ, 231, 854
Backer, D. C. 1970a, Nature, 227, 692
Backer, D. C. 1970b, Nature, 228, 752
Bai, X., & Spitkovsky, A. 2010, ApJ, 715, 1282
Beloborodov, A. M. 2008, ApJ, 683, L41
Beskin, V. S. 2010, MHD Flows in Compact Astrophysical Objects: Accretion, Winds and Jets (Berlin: Springer)
Bhattacharyya, B., Gupta, Y., & Gil, J. 2008, MNRAS, 383, 1538
Bhattacharyya, B., Gupta, Y., Gil, J., & Sendyk, M. 2007, MNRAS, 377, L10
Biggs, J. D., McCulloch, P. M., Hamilton, P. A., Manchester, R. N., & Lyne, A. G. 1985, MNRAS, 215, 281
Champion, D. J., Lorimer, D. R., McLaughlin, M. A., et al. 2005, MNRAS, 363, 929
Cheng, A., Ruderman, M., & Sutherland, P. 1976, ApJ, 203, 209
Clemens, J. C., & Rosen, R. 2004, ApJ, 609, 340
Cordes, J. M. 1978, ApJ, 222, 1006
Daugherty, J. K., & Harding, A. K. 1982, ApJ, 252, 337
Deshpande, A. A., & Rankin, J. M. 1999, ApJ, 524, 1008
Drake, F. D., & Craft, H. D. 1968, Nature, 220, 231
Durdin, J. M., Large, M. I., Little, A. G., et al. 1979, MNRAS, 186, 39P
Esamdin, A., Lyne, A. G., Graham-Smith, F., et al. 2005, MNRAS, 356, 59
Fung, P. K., Khechinashvili, D., & Kuijpers, J. 2006, A&A, 445, 779
Gil, J., Melikidze, G. I., & Geppert, U. 2003, A&A, 407, 315
Gil, J. A., & Sendyk, M. 2000, ApJ, 541, 351
Gogoberidze, G., Machabeli, G. Z., Melrose, D. B., & Luo, Q. 2005, MNRAS, 360, 669
Goldreich, P., & Julian, W. H. 1969, ApJ, 157, 869
Gupta, Y., Gil, J., Kijak, J., & Sendyk, M. 2004, A&A, 426, 229
Harding, A. K., & Muslimov, A. G. 1998, ApJ, 508, 328
Hewish, A., Bell, S. J., Pilkington, J. D. H., Scott, P. F., & Collins, R. A. 1968, Nature, 217, 709
Hibschman, J. A., & Arons, J. 2001, ApJ, 554, 624
Hobbs, G., Lyne, A. G., Kramer, M., Martin, C. E., & Jordan, C. 2004, MNRAS, 353, 1311
Janssen, G. H., & van Leeuwen, J. 2004, A&A, 425, 255
Kalapotharakos, C., Kazanas, D., Harding, A., & Contopoulos, I. 2012, ApJ, 749, 2
Kloumann, I. M., & Rankin, J. M. 2010, MNRAS, 408, 40
Kuijpers, J. M. E. 2009, in Neutron Stars and Pulsars, ed. W. Becker (Astrophysics and Space Science Library, Vol. 357; Berlin: Springer), 543
Levinson, A., Melrose, D., Judge, A., & Luo, Q. 2005, ApJ, 631, 456
Li, J., Spitkovsky, A., & Tchekhovskoy, A. 2012, ApJ, 746, 60
Lyne, A. G., & Manchester, R. N. 1988, MNRAS, 234, 477
Manchester, R. N., Lyne, A. G., Camilo, F., et al. 2001, MNRAS, 328, 17
Manchester, R. N., Lyne, A. G., Taylor, J. H., et al. 1978, MNRAS, 185, 409
Rankin, J. M., & Suleymanova, S. A. 2006, A&A, 453, 679
Redman, S. L., Wright, G. A. E., & Rankin, J. M. 2005, MNRAS, 357, 859
Ruderman, M. A., & Sutherland, P. G. 1975, ApJ, 196, 51
Scharlemann, E. T., Arons, J., & Fawley, W. M. 1978, ApJ, 222, 297
Schiff, L. I. 1939, Proc. Natl Acad. Sci., 25, 391
Serylak, M. 2011, PhD thesis, Univ. Amsterdam, http://dare.uva.nl/en/record/369352
Smits, J. M., Mitra, D., & Kuijpers, J. 2005, A&A, 440, 683
Sturrock, P. A. 1971, ApJ, 164, 529
Timokhin, A. N. 2006, MNRAS, 368, 1055
Timokhin, A. N. 2007a, MNRAS, 379, 605
Timokhin, A. N. 2007b, Ap&SS, 308, 575
Timokhin, A. N. 2007c, Ap&SS, 308, 345
Timokhin, A. N. 2010a, MNRAS, 408, L41
Timokhin, A. N. 2010b, MNRAS, 408, 2092
van Leeuwen, A. G. J., Kouwenhoven, M. L. A., Ramachandran, R., Rankin, J. M., & Stappers, B. W. 2002, A&A, 387, 169
van Leeuwen, A. G. J., Stappers, B. W., Ramachandran, R., & Rankin, J. M. 2003, A&A, 399, 223
Weltevrede, P., Edwards, R. T., & Stappers, B. W. 2006, A&A, 445, 243
Weltevrede, P., Stappers, B. W., & Edwards, R. T. 2007, A&A, 469, 607
Wright, G. A. E. 2003, MNRAS, 344, 1041